Analytical preconditioners for Neumann elastodynamic Boundary Element Methods

Stéphanie Chaillat, Marion Darbas, Frédérique Le Louër

Analytical preconditioners for Neumann elastodynamic Boundary Element Methods

Stéphanie Chaillat[a], Marion Darbas[b,*], Frédérique Le Louër[c]

[a] *Laboratoire POEMS (CNRS-INRIA-ENSTA), Institut Polytechnique de Paris, ENSTA-UMA, 828 Bd des Maréchaux, 91762 Palaiseau Cedex, FRANCE*
[b] *LAMFA UMR CNRS 7352 Université de Picardie Jules Verne, 33 rue Saint-Leu 80039 Amiens Cedex, FRANCE*
[c] *LMAC EA 2222 Sorbonne Universités, Université de technologie de Compiègne, CS 60 319 - 60 203 Compiègne cedex, FRANCE*

Abstract

Recent works in the Boundary Element Method (BEM) community have been devoted to the derivation of fast techniques to perform the matrix vector product needed in the iterative solver. Fast BEMs are now very mature. However, it has been shown that the number of iterations can significantly hinder the overall efficiency of fast BEMs. The derivation of robust preconditioners is now inevitable to increase the size of the problems that can be considered. Analytical preconditioners offer a very interesting strategy by improving the spectral properties of the boundary integral equations ahead from the discretization.

The main contribution of this paper is to propose new analytical preconditioners to treat Neumann exterior scattering problems in 2D and 3D elasticity. These preconditioners are local approximations of the adjoint Neumann-to-Dirichlet map. We propose three approximations with different orders. The resulting boundary integral equations are preconditioned Combined Field Integral Equations (CFIEs). An analytical spectral study confirms the expected behavior of the preconditioners, i.e., a better eigenvalue clustering especially in the elliptic part contrary to the standard CFIE of the first-kind. We provide various 2D numerical illustrations of the efficiency of the method for different smooth and non smooth geometries. In particular, the number of iterations is shown to be independent of the density of discretization points per wavelength which is not the case of the standard CFIE. In addition, it is less sensitive to the frequency.

Keywords: Scattering, time-harmonic elastic waves, Boundary Element Method, analytical preconditioner, approximate local Neumann-to-Dirichlet map, cavity.

1. Introduction

The development of numerical methods for solving highly oscillatory elastic problems is of great interest in medical or industrial applications (for example elastrography imaging, seismology, geophysical exploration or non-destructive testing). This paper considers the solution of scattering problems of time-harmonic elastic waves by a two- or three-dimensional bounded obstacle with a Neumann boundary condition. Various numerical approaches exist to deal with exterior boundary-value problems [59]. We mention spectral methods [24, 44, 49], Finite Element Methods [41, 9] or Finite Difference Methods [56, 39]. For the class of volume methods, the unbounded computational domain must be truncated using an artificial boundary at a finite distance on which a boundary condition is imposed. Many possibilities are proposed in the literature: nonreflecting boundary conditions [38, 37] such as Absorbing Boundary Conditions (ABCs) [29, 18, 34] or Perfectly

*Corresponding author
Email addresses: stephanie.chaillat@ensta-paristech.fr (Stéphanie Chaillat), marion.darbas@u-picardie.fr (Marion Darbas), frederique.le-louer@utc.fr (Frédérique Le Louër)

Matched Layers (PMLs) [8, 40, 26]. The method of boundary integral equations (BIEs) is another classical tool for solving scattering problems of time-harmonic waves in unbounded, homogeneous and isotropic media (see e.g. [10, 42, 48, 47]). The main advantage is to formulate the exterior boundary value-problem as an integral equation on the boundary of the scatterer. Only the surface of the obstacle is thus needed to be meshed in contrast to volume methods and the dimensionality of the problem is reduced by one. However, the discretization matrix of a boundary integral operator is dense. Furthermore, in order to capture the oscillatory phenomenon, one has to fix typically about ten discretization points per wavelength per dimension. The solution of these large and fully-populated complex linear systems is handled by iterative solvers, namely GMRES [60]. The standard Boundary Element Method (BEM) results in high computational costs in terms of computational time ($\mathcal{O}(N^2)$ per iteration) and memory requirements ($\mathcal{O}(N^2)$), where N denotes the number of degrees of freedom (DOFs) of the BEM model. A number of algorithms has been introduced to evaluate matrix-vector products in a fast way, when the matrix is obtained by the discretization of an integral operator. The Fast Multipole accelerated Boundary Element Method (FM-BEM) is one of the efficient methods. The method has been introduced by Rokhlin [55] and extended to various domains included 3D elastodynamics [20, 19]. A different kind of compression can be obtained by applying the adaptive cross approximation (ACA) algorithm and hierarchical matrices [7]. In addition, the spectral properties of the most stable integral equation formulations, the Combined Field Integral Equations (CFIEs), are usually not well suited for Krylov-subspace iterative solvers such as GMRES. The cavity problem is particularly challenging because the standard CFIE is a boundary integral equation of the first kind for such a boundary condition. It involves the boundary Neumann trace of the double-layer potential which is a pseudodifferential operator of order 1. Consequently, a sequence of corresponding eigenvalues tends to infinity. The condition number of the matrix behaves like $\mathcal{O}(1/h)$ in the standard basis where h is the mesh size. We will see that this drawback of the CFIE is exacerbated at high frequencies. In this paper, we focus on the construction of new well-conditioned BIEs which are more robust than the standard CFIE.

Specifically, two families of preconditioners exist. We can cite algebraic preconditioning approaches such as incomplete LU, SParse Approximative Inverse [16, 17], multi-grid methods [15], nested GMRES algorithm [23] which have been applied to electromagnetic or elastodynamic FM-BEMs. However, since algebraic preconditioners retain only a small contribution of the system matrix, they do not contain enough information on the underlying continuous operator. This approach is performant but shows only moderate efficiency for high frequency problems. Analytical preconditioners offer a very interesting alternative. They act ahead from the discretization. This preconditioning technique based on boundary integral operators of opposite orders, also known as Calderón's preconditioning, has been introduced by Steinbach and Wendland [57] in electromagnetism. Since then, several works have been devoted to the derivation of Fredholm boundary integral equations of the second kind for both acoustic and electromagnetic scattering problems by closed surfaces (e.g. [4, 5, 50, 51, 1, 12, 13, 31, 11, 54, 25, 35, 58, 36]) or open surfaces (e.g. [27, 28, 3, 14]). Among them, approximations of the Dirichlet-to-Neumann map (respectively the Neumann-to-Dirichlet map) naturally define robust analytical preconditioners when considering Dirichlet (respectively Neumann) boundary value-problems. They are introduced as regularizing operators in the integral representation of the scattered field and improve the spectral properties of the resulting boundary integral equations. A pseudo inverse of the principal classical symbol of the single layer boundary integral operator - or equivalently the principal classical symbol of the Neumann trace of the double layer boundary integral operator - is used to approach the Dirichlet-to-Neumann map and its adjoint operator [6, 5, 30] in the framework of the On-Surface Radiation Condition (OSRC) methods (e.g. [46, 43, 2]). In acoustics, the resulting preconditioner is expressed analytically by a simple square-root of the form $i\kappa(\mathrm{I} + \Delta_\Gamma/\kappa^2)^{1/2}$ where κ is the wavenumber and Δ_Γ the Laplace-Beltrami operator. Using same techniques of pseudodifferential calculus, recent works have proposed analytical preconditioners for Dirichlet elastic BEM [32]. Some difficulties inherent to elasticity have to be overcome. For the elasticity case, the double layer boundary integral operator and its adjoint are not compact even for sufficiently smooth boundaries. This

implies, according to Calderón's identities, that regularizing the standard BIEs via a pseudo inverse of the single layer boundary integral operator is not sufficient to obtain well-conditioned boundary integral equations. The principal part of the double layer boundary integral operator has also to be taken into account in the preconditioner to regularize the single layer integral operator. It is not an easy task to obtain the expressions of the principal parts of each elementary boundary integral operator. To this end, a modified potential theory is applied and the tangential Günter derivative plays an important role. The approximations of the Dirichlet-to-Neumann map are expressed in terms of surface differential operators, square-root operators and their inverse. These preconditioners can easily be combined with fast methods such as FMM [31], and yield a very fast convergence of GMRES solver and in particular with a number of iterations independent of the frequency and the mesh density.

In this paper, we construct analytical preconditioners for the iterative solution of cavity problems. To the best of our knowledge, this is the first contribution in this sense in 3D elastodynamics. Contrary to the acoustic and electromagnetic cases, the definition of the Neumann-to-Dirichlet preconditioner as the inverse of the Dirichlet-to-Neumann preconditioner is not sufficient to construct well-conditioned BIEs for Neumann scattering problems. The approximations of different orders of the adjoint Neumann-to-Dirichlet map, that we propose to apply as regularizing operators, are derived using strategies developed in [32]. However, we can no more use the modified potential theory and the help of the tangential Günter derivative to overcome the non-compactness of the boundary double-layer integral operator.

The paper is organized as follows: in Section 2, we introduce the problem setting. We present the Combined Field Integral Equation (CFIE) formulations that are numerically investigated in this paper. In Section 3, we describe the different approximate adjoint Neumann-to-Dirichlet maps and the corresponding CFIEs in the two- and three-dimensional cases. Section 4 is devoted to analytical investigations of the spectral properties of the standard and preconditioned operators in the particular case of the elastic sphere. Furthermore, we study the effect of both the number of spherical harmonics and the frequency increase on the condition number. In Section 5, we provide some elements of the discretization and implementation. We also give various numerical illustrations of the efficiency of the method for different 2D geometries. We address numerical investigation of the eigenvalues of the classical and preconditioned CFIEs. Finally, we draw concluding remarks, and we discuss possible research lines in Section 6.

2. The Navier exterior problem and standard boundary integral equations

2.1. The Navier exterior problem

We consider an elastic cavity represented by a bounded domain Ω^- in $\mathbb{R}^d$, $d = 2, 3$, with a closed boundary $\Gamma := \partial\Omega^-$ of class $\mathscr{C}^2$ at least. Let Ω^+ denote the exterior domain $\mathbb{R}^d \backslash \overline{\Omega^-}$ and $\boldsymbol{n}$ the outer unit normal vector to the boundary Γ. The Lamé parameters μ and λ and the density ρ are positive constants. The propagation of time-harmonic waves in an isotropic and homogeneous elastic medium is governed by the Navier equation [48, Eq. (12.5) page 55]

$$\mu \boldsymbol{\Delta} \boldsymbol{u} + (\lambda + \mu) \boldsymbol{\nabla} \operatorname{div} \boldsymbol{u} + \rho \omega^2 \boldsymbol{u} = 0, \tag{1a}$$

where $\omega > 0$ denotes the angular frequency. The displacement field $\boldsymbol{u}$ is decomposed into a longitudinal field $\boldsymbol{u}_p$ (compressional part) with vanishing curl and a transverse divergence-free field $\boldsymbol{u}_s$, both solutions to the Helmholtz equation with respective wavenumbers $\kappa_p^2 = \rho\omega^2(\lambda + 2\mu)^{-1}$ and $\kappa_s^2 = \rho\omega^2\mu^{-1}$. The Neumann trace, defined by $\boldsymbol{t}_{|\Gamma} := \boldsymbol{T}\boldsymbol{u}$, is given by the traction operator

$$\boldsymbol{T} = 2\mu \frac{\partial}{\partial \boldsymbol{n}} + \lambda \boldsymbol{n} \operatorname{div} + \mu \, \boldsymbol{n} \times \mathbf{curl}\,.$$

The two-dimensional traction is obtained by setting $\boldsymbol{u} = (u_1, u_2, 0)$ and $\boldsymbol{n} = (n_1, n_2, 0)$ in the above definition.

The elastic cavity problem is formulated as follows : Given an incident displacement wave $\boldsymbol{u}^{inc}$ which is assumed to solve the Navier equation in the absence of any scatterer, find the scattered field $\boldsymbol{u}$ to the Navier equation (1a) in Ω^+ which satisfies the Neumann boundary condition

$$\boldsymbol{t}_{|\Gamma} = -\boldsymbol{t}^{inc}_{|\Gamma} \quad \text{on } \Gamma, \tag{1b}$$

where we have set $\boldsymbol{t}^{inc}_{|\Gamma} = \boldsymbol{T}\boldsymbol{u}^{inc}$. In addition, the behavior of the scattered displacement field $\boldsymbol{u}$ at infinity is described by the Kupradze radiation conditions [48, Eqs (2.6)-(2.9) page 126]

$$\lim_{r\to\infty} r\left(\frac{\partial \boldsymbol{u}_p}{\partial r} - i\kappa_p \boldsymbol{u}_p\right) = 0, \qquad \lim_{r\to\infty} r\left(\frac{\partial \boldsymbol{u}_s}{\partial r} - i\kappa_s \boldsymbol{u}_s\right) = 0, \quad r = |\boldsymbol{x}|, \tag{1c}$$

uniformly in all directions.

We denote by $H^s_{loc}(\overline{\Omega^+})$ and $H^s(\Gamma)$ the standard (local in the case of the exterior domain) complex valued, Hilbert-Sobolev spaces of order $s \in \mathbb{R}$ defined on $\overline{\Omega^+}$ and Γ respectively (with the convention $H^0 = L^2$). Spaces of vector functions will be denoted by boldface letters, thus $\boldsymbol{H}^s = (H^s)^d$. We set $\Delta^*\boldsymbol{u} := \mu\boldsymbol{\Delta}\boldsymbol{u} + (\lambda+\mu)\boldsymbol{\nabla}\operatorname{div}\boldsymbol{u}$. The radiating solution to (1a)-(1b)-(1c) belongs to the space

$$\boldsymbol{H}^1_+(\Delta^*) := \boldsymbol{H}^1_{loc}(\Omega^+, \Delta^*) := \left\{\boldsymbol{u} \in \boldsymbol{H}^1_{loc}(\overline{\Omega^+}) : \ \Delta^*\boldsymbol{u} \in \boldsymbol{L}^2_{loc}(\overline{\Omega^+})\right\}.$$

For existence and uniqueness results, we refer to Kupradze [47, 48].

2.2. Potential theory and integral representation

The first main difficulty arising in the numerical solution to the exterior boundary value-problem (1a)-(1b)-(1c) is related to the unbounded computational domain Ω^+. Integral equation based methods are one of the possible tools to overcome this issue. For any positive real number κ, let

$$G(\kappa, \boldsymbol{x}-\boldsymbol{y}) = \begin{cases} \dfrac{i}{4}H^{(1)}_0(\kappa|\boldsymbol{x}-\boldsymbol{y}|) & \text{if } d=2, \\ \dfrac{e^{i\kappa|\boldsymbol{x}-\boldsymbol{y}|}}{4\pi|\boldsymbol{x}-\boldsymbol{y}|}, \boldsymbol{x}\neq\boldsymbol{y}, & \text{if } d=3, \end{cases}$$

be the fundamental solution of the Helmholtz equation $\Delta v + \kappa^2 v = 0$. The fundamental solution of the Navier equation is written

$$\Phi(\boldsymbol{x},\boldsymbol{y}) = \frac{1}{\mu}\left[G(\kappa_s, |\boldsymbol{x}-\boldsymbol{y}|)\cdot \mathrm{I}_{\mathbb{R}^d} + \frac{1}{\kappa_s^2}\boldsymbol{\nabla}^{\boldsymbol{x}}\boldsymbol{\nabla}^{\boldsymbol{x}\,\mathsf{T}}\big(G(\kappa_s,|\boldsymbol{x}-\boldsymbol{y}|) - G(\kappa_p,|\boldsymbol{x}-\boldsymbol{y}|)\big)\right]. \tag{2}$$

The single- and double-layer potential operators are defined by

$$\mathcal{S}\boldsymbol{\varphi} = \int_\Gamma \Phi(\cdot\,,\boldsymbol{y})\boldsymbol{\varphi}(\boldsymbol{y})ds(\boldsymbol{y}) \quad \text{and} \quad \mathcal{D}\boldsymbol{\psi} = \int_\Gamma [\boldsymbol{T}_{\boldsymbol{y}}\Phi(\cdot\,,\boldsymbol{y})]^{\mathsf{T}}\boldsymbol{\psi}(\boldsymbol{y})ds(\boldsymbol{y}), \tag{3}$$

where $\boldsymbol{T}_{\boldsymbol{y}} = \boldsymbol{T}(\boldsymbol{n}(\boldsymbol{y}), \partial_{\boldsymbol{y}})$ and $\boldsymbol{T}_{\boldsymbol{y}}\Phi(\boldsymbol{x},\boldsymbol{y})$ is the tensor obtained by applying the traction operator $\boldsymbol{T}_{\boldsymbol{y}}$ to each column of $\Phi(\boldsymbol{x},\boldsymbol{y})$. For a solution $\boldsymbol{u}$ of the Navier equation (1a) in Ω^+, that satisfies the Kupradze radiation conditions, one can derive the Somigliana integral representation formula: for $\boldsymbol{x} \in \Omega^+$

$$\boldsymbol{u}(\boldsymbol{x}) = \mathcal{D}\boldsymbol{u}_{|\Gamma}(\boldsymbol{x}) - \mathcal{S}\boldsymbol{t}_{|\Gamma}(\boldsymbol{x}). \tag{4}$$

The Cauchy data $(\boldsymbol{u}_{|\Gamma}, \boldsymbol{t}_{|\Gamma})$ become the new unknowns of the problem. The displacement field $\boldsymbol{u}$ in Ω^+ is uniquely determined from the knowledge of these two surface fields.

Given vector densities $\boldsymbol{\varphi}$ and $\boldsymbol{\psi}$, the boundary integral operators S, D, D' and N are defined,

for $\boldsymbol{x} \in \Gamma$, by

$$\begin{aligned} S\boldsymbol{\varphi}(\boldsymbol{x}) &= \int_\Gamma \Phi(\boldsymbol{x},\boldsymbol{y})\boldsymbol{\varphi}(\boldsymbol{y})\, ds(\boldsymbol{y}), \\ D\boldsymbol{\psi}(\boldsymbol{x}) &= \int_\Gamma [\boldsymbol{T}_{\boldsymbol{y}}\Phi(\boldsymbol{x},\boldsymbol{y})]^{\mathsf{T}}\boldsymbol{\psi}(\boldsymbol{y})\, ds(\boldsymbol{y}), \\ D^{'}\boldsymbol{\varphi}(\boldsymbol{x}) &= \int_\Gamma \boldsymbol{T}_{\boldsymbol{x}}\left\{\Phi(\boldsymbol{x},\boldsymbol{y})\boldsymbol{\varphi}(\boldsymbol{y})\right\}\, ds(\boldsymbol{y}), \\ N\boldsymbol{\psi}(\boldsymbol{x}) &= \int_\Gamma \boldsymbol{T}_{\boldsymbol{x}}\left\{[\boldsymbol{T}_{\boldsymbol{y}}\Phi(\boldsymbol{x},\boldsymbol{y})]^{\mathsf{T}}\boldsymbol{\psi}(\boldsymbol{y})\right\}\, ds(\boldsymbol{y}). \end{aligned}$$

By applying the exterior Dirichlet and Neumann traces to $\mathcal{S}$ and $\mathcal{D}$ we have [32]

$$\begin{aligned} (\mathcal{S}\boldsymbol{\varphi})_{|\Gamma} = S\boldsymbol{\varphi}, \quad \left(\boldsymbol{T}\mathcal{S}\boldsymbol{\varphi}\right)_{|\Gamma} = -\frac{1}{2}\boldsymbol{\varphi} + D^{'}\boldsymbol{\varphi}, \\ (\mathcal{D}\boldsymbol{\psi})_{|\Gamma} = \frac{1}{2}\boldsymbol{\psi} + D\boldsymbol{\psi}, \quad \text{and } \left(\boldsymbol{T}\mathcal{D}\boldsymbol{\psi}\right)_{|\Gamma} = N\boldsymbol{\psi}, \end{aligned} \tag{5}$$

where I is the identity operator. The operator S is a pseudo-differential operator of order -1, i.e it is bounded from $\boldsymbol{H}^{-\frac{1}{2}}(\Gamma)$ to $\boldsymbol{H}^{\frac{1}{2}}(\Gamma)$ and compact from $\boldsymbol{H}^{-\frac{1}{2}}(\Gamma)$ to itself. The operator D and its adjoint $D^{'}$ are of order 0, i.e. they have a strongly singular kernel and are bounded from $\boldsymbol{H}^{\frac{1}{2}}(\Gamma)$ and $\boldsymbol{H}^{-\frac{1}{2}}(\Gamma)$ to themselves, respectively. The operator N is of order 1, i.e. it has a hypersingular kernel and is bounded from $\boldsymbol{H}^{\frac{1}{2}}(\Gamma)$ to $\boldsymbol{H}^{-\frac{1}{2}}(\Gamma)$. The Calderón projectors for the time-harmonic Navier equation are

$$P^{\pm} = \begin{pmatrix} \pm\frac{1}{2}\mathrm{I} + D & -S \\ N & \pm\frac{1}{2}\mathrm{I} - D' \end{pmatrix}.$$

We have $P^{+} \circ P^{-} = P^{-} \circ P^{+} = 0$ and thus the relations

$$\begin{aligned} SD' = DS\,, \quad D'N = ND\,, \\ SN = D^2 - \frac{1}{4}\mathrm{I}\,, \quad NS = D'^2 - \frac{1}{4}\mathrm{I}. \end{aligned} \tag{6}$$

2.3. Standard Boundary Integral Equations

There exists various possible boundary integral equations to obtain the Cauchy data $(\boldsymbol{u}_{|\Gamma}, \boldsymbol{t}_{|\Gamma})$. We focus on combined field boundary integral equations that admit the unique solvability property. The Neumann trace $\boldsymbol{t}_{|\Gamma}$ is known through the boundary condition (1b).

We consider the direct method based on the following integral representation formula

$$\boldsymbol{u} = \mathcal{D}\big(\boldsymbol{u}_{|\Gamma} + \boldsymbol{u}^{inc}_{|\Gamma}\big)\,.$$

Taking the exterior Dirichlet and Neumann traces of the right hand side, we obtain on Γ

$$(\frac{\mathrm{I}}{2} + D)\big(\boldsymbol{u}_{|\Gamma} + \boldsymbol{u}^{inc}_{|\Gamma}\big) = \boldsymbol{u}_{|\Gamma} \Leftrightarrow (\frac{\mathrm{I}}{2} - D)\big(\boldsymbol{u}_{|\Gamma} + \boldsymbol{u}^{inc}_{|\Gamma}\big) = \boldsymbol{u}^{inc}_{|\Gamma} \quad \text{and} \quad N\big(\boldsymbol{t}_{|\Gamma} + \boldsymbol{t}^{inc}_{|\Gamma}\big) = \boldsymbol{t}_{|\Gamma} = -\boldsymbol{t}^{inc}_{|\Gamma}.$$

Combining the previous two equations, we construct the standard CFIE: find the physical unknown $\psi = \boldsymbol{u}_{|\Gamma} + \boldsymbol{u}^{inc}_{|\Gamma} \in \boldsymbol{H}^{\frac{1}{2}}(\Gamma)$ solution to

$$(\frac{\mathrm{I}}{2} - D - i\eta N)\psi = \boldsymbol{u}^{inc}_{|\Gamma} + i\eta\boldsymbol{t}^{inc}_{|\Gamma}, \quad \text{on } \Gamma, \tag{7}$$

with η a coupling parameter. The integral equation (7) is well-posed for any frequency ω and

any non-zero real parameter η [42, 47, 48]. However, it involves the boundary integral operator N which is a pseudodifferential operator of order 1. Thus, this boundary integral equation is of the first-kind and admits a countable set of eigenvalues that tends to infinity. We will see that this standard CFIE is not well-suited for iterative solvers, particularly at high frequencies (see Sections 4 and 5). This motivates the research of new and well-conditioned CFIEs.

3. Analytical preconditioners and regularized CFIE

3.1. Principle of analytical preconditioners

The analytical preconditioning technique consists in first constructing local approximations of the exact exterior Neumann-to-Dirichlet operator. Secondly, we use them to get new CFIEs with interesting spectral properties. The principle of the approach is the following.

Consider the exact exterior Neumann-to-Dirichlet operator (called NtD)

$$\boldsymbol{V}^{\mathrm{ex}} : \boldsymbol{t}_{|\Gamma} \in \boldsymbol{H}^{-\frac{1}{2}}(\Gamma) \mapsto \boldsymbol{V}^{\mathrm{ex}}\boldsymbol{t}_{|\Gamma} := \boldsymbol{u}_{|\Gamma} \in \boldsymbol{H}^{\frac{1}{2}}(\Gamma)\,. \tag{8}$$

We write the Somigliana integral representation formula (4) of the scattered field under the form

$$\boldsymbol{u}(\boldsymbol{x}) = \mathcal{D}\boldsymbol{u}_{|\Gamma}(\boldsymbol{x}) - \mathcal{S}\boldsymbol{t}_{|\Gamma}(\boldsymbol{x}) = \mathcal{D}\boldsymbol{V}^{\mathrm{ex}}\boldsymbol{t}_{|\Gamma}(\boldsymbol{x}) - \mathcal{S}\boldsymbol{t}_{|\Gamma}(\boldsymbol{x}),\ \boldsymbol{x} \in \Omega^{+}. \tag{9}$$

We take the exterior Neumann trace of the representation (9)

$$\boldsymbol{t}_{|\Gamma}(\boldsymbol{x}) = \big(N\boldsymbol{V}^{\mathrm{ex}} + \frac{\mathrm{I}}{2} - D'\big)\boldsymbol{t}_{|\Gamma}(\boldsymbol{x}),\ \boldsymbol{x} \in \Gamma,$$

and hence the exact NtD operator $\boldsymbol{V}^{\mathrm{ex}}$ satisfies on Γ

$$\frac{\mathrm{I}}{2} - D' + N\boldsymbol{V}^{\mathrm{ex}} = \mathrm{I}.$$

In order to avoid the use of non-physical quantities, we consider the L^2-adjoint form of the above-written boundary integral equation operator

$$\frac{\mathrm{I}}{2} - D + \boldsymbol{V}^{\mathrm{ex}'}N = \mathrm{I}, \tag{10}$$

that is related to the CFIE (7). Thus we conclude that the adjoint NtD $\boldsymbol{V}^{\mathrm{ex}'}$ is an ideal analytical preconditioner for the CFIE, in the sense that the use of $\boldsymbol{V}^{\mathrm{ex}'}$ (instead of the constant η) to regularize the operator N gives directly the solution of the scattering problem. Furthermore, assume that ω is not an eigenfrequency of the Navier equation (1a) in Ω^{-} with a Neumann homogeneous boundary condition, we deduce from relation (10) that the adjoint NtD map is expressed in terms of elementary boundary integral operators on Γ by

$$\boldsymbol{V}^{\mathrm{ex}'} = N^{-1}\Big(\frac{\mathrm{I}}{2} + D\Big). \tag{11}$$

The Calderon formula $SN = D^2 - \dfrac{1}{4}\mathrm{I}$ (see (6)) leads to another integral representation

$$\boldsymbol{V}^{\mathrm{ex}'} = -S\Big(\frac{\mathrm{I}}{2} - D\Big)^{-1}. \tag{12}$$

However, it is too expensive numerically to apply one of these representations of the operator $\boldsymbol{V}^{\mathrm{ex}'}$ as a preconditioner for the CFIE. Instead, an approximation $\boldsymbol{V}'$ of $\boldsymbol{V}^{\mathrm{ex}'}$ is introduced to construct

a preconditioned CFIE : Find the total field $\psi = \boldsymbol{u}_{|\Gamma} + \boldsymbol{u}^{inc}_{|\Gamma} \in \boldsymbol{H}^{\frac{1}{2}}(\Gamma)$ solution to

$$(\frac{\mathrm{I}}{2} - D + \boldsymbol{V}'N)\boldsymbol{\psi} = \boldsymbol{u}^{inc}_{|\Gamma} - \boldsymbol{V}'\boldsymbol{t}^{inc}_{|\Gamma}, \quad \text{on } \Gamma. \tag{13}$$

The spectral properties of (13) depend on the choice of the approximate adjoint NtD map $\boldsymbol{V}'$.

3.2. Three-dimensional case

In this subsection, we give the expressions of different approximations of the adjoint NtD map and their corresponding preconditioned CFIEs. First, let us introduce the expressions of the principal parts of the operators S and D using tools proposed in [32]. The operator $P(S)$ is decomposed into two terms: $P(S) = S_1 + S_2$ with

$$\begin{aligned} S_1 &= \frac{i}{2\rho\omega^2}\Big(\boldsymbol{n}\big(\Delta_\Gamma + \kappa_p^2\mathrm{I}\big)^{\frac{1}{2}}\boldsymbol{n}\cdot\mathrm{I}_{\boldsymbol{n}} + \boldsymbol{\tau}\big(\Delta_\Gamma + \kappa_s^2\mathrm{I}\big)^{\frac{1}{2}}\boldsymbol{\tau}\cdot\mathrm{I}_{\boldsymbol{\tau}}\Big) \\ S_2 &= -\frac{i}{2\rho\omega^2}\Big(\boldsymbol{n}\,\Delta_\Gamma\big(\Delta_\Gamma + \kappa_s^2\mathrm{I}\big)^{-\frac{1}{2}}\boldsymbol{n}\cdot\mathrm{I}_{\boldsymbol{n}} + \boldsymbol{\nabla}_\Gamma\big(\Delta_\Gamma + \kappa_p^2\mathrm{I}\big)^{-\frac{1}{2}}\mathrm{div}_\Gamma\,\mathrm{I}_{\boldsymbol{\tau}}\Big) \end{aligned} \tag{14}$$

where $\mathrm{I}_{\boldsymbol{n}} = \boldsymbol{n}\otimes\boldsymbol{n}$ and $\mathrm{I}_{\boldsymbol{\tau}} = \mathrm{I} - \mathrm{I}_{\boldsymbol{n}}$. We refer to [53, pages 68-75] for the definition of the surface differential operators: the tangential gradient $\boldsymbol{\nabla}_\Gamma$, the surface divergence div_Γ and the scalar Laplace-Beltrami operator Δ_Γ. The square-root $z^{1/2}$ of a complex number z stands for the classical complex square-root with branch-cut along the negative real axis. The operator $P(D)$ is also decomposed into two terms: $P(D) = D_1 + D_2$ with

$$\begin{aligned} D_1 &= \frac{i}{2}\Big(\boldsymbol{n}\big(\Delta_\Gamma + \kappa_p^2\mathrm{I}\big)^{-\frac{1}{2}}\mathrm{div}_\Gamma\,\mathrm{I}_{\boldsymbol{t}} - \boldsymbol{\nabla}_\Gamma\big(\Delta_\Gamma + \kappa_s^2\mathrm{I}\big)^{-\frac{1}{2}}\boldsymbol{n}\cdot\mathrm{I}_{\boldsymbol{n}}\Big) \\ D_2 &= \frac{i\mu}{\rho\omega^2}\Big(-\boldsymbol{n}\big(\Delta_\Gamma + \kappa_s^2\mathrm{I}\big)^{\frac{1}{2}}\mathrm{div}_\Gamma\,\mathrm{I}_{\boldsymbol{t}} + \boldsymbol{n}\Delta_\Gamma\big(\Delta_\Gamma + \kappa_p^2\mathrm{I}\big)^{-\frac{1}{2}}\mathrm{div}_\Gamma\,\mathrm{I}_{\boldsymbol{t}} \\ &\qquad + \boldsymbol{\nabla}_\Gamma\big(\Delta_\Gamma + \kappa_p^2\mathrm{I}\big)^{\frac{1}{2}}\big(\boldsymbol{n}\cdot\mathrm{I}_{\boldsymbol{n}}\big) - \boldsymbol{\nabla}_\Gamma\big(\Delta_\Gamma + \kappa_s^2\mathrm{I}\big)^{-\frac{1}{2}}\Delta_\Gamma\,\big(\boldsymbol{n}\cdot\mathrm{I}_{\boldsymbol{n}}\big)\Big). \end{aligned} \tag{15}$$

From (12)-(14)-(15), we derive several approximations of the adjoint NtD map.

Low-order approximation. We retain in (14) the informations associated to the first eigenmode of the operators only. We obtain the following adjoint NtD approximation

$$\boldsymbol{V}' := \boldsymbol{V}'_{\mathrm{LO}} = -i\Big(\frac{1}{(\lambda+2\mu)\kappa_p}\mathrm{I}_{\boldsymbol{n}} + \frac{1}{\mu\kappa_s}\mathrm{I}_{\boldsymbol{t}}\Big). \tag{16}$$

Importantly, the operator (16) is only coming from S_1 (14).This low-order approximation is the equivalent in elasticity of the zeroth-order approximation $1/(i\kappa)$ of the acoustic NtD map where κ is the wavenumber. The associated preconditioned integral equation is given by

$$(\frac{\mathrm{I}}{2} - D + \boldsymbol{V}'_{\mathrm{LO}}N)\boldsymbol{\psi} = \boldsymbol{u}^{inc}_{|\Gamma} - \boldsymbol{V}'_{\mathrm{LO}}\boldsymbol{t}^{inc}_{|\Gamma}, \quad \text{on } \Gamma, \tag{17}$$

and is called *LO-preconditioned CFIE* (LO P-CFIE) in the remaining of the paper. The main advantage of this preconditioner is to be very easy to implement. This new boundary integral equation can be interpreted as the equivalent in elasticity of the usual CFIE with the optimal coupling parameter of Kress [45] in acoustics. By construction, the approximation (16) provides a good clustering of the first eigenvalues (associated with propagating modes) only. We will show that we need high-order approximations to regularize the operator N of order 1 and then to cluster eigenvalues associated with evanescent modes (see Sections 4 and 5).

High-order approximation. Similarly to previous works [32, 22] realised for the Dirichlet boundary condition case, we propose to consider the two following high-order approximations of the adjoint NtD map

$$\boldsymbol{V}'_{\mathrm{HO}(1)} = -2P(S) \tag{18}$$

$$\boldsymbol{V}'_{\mathrm{HO}(2)} = -P(S)\Big(\frac{\mathrm{I}}{2} - P(D)\Big)^{-1} \tag{19}$$

where $P(S)$ and $P(D)$ are the respective principal parts of the operators S and D. For a numerical purpose, these approximations are preferred to the one of (11) that involves the principal part of the operator N^{-1}. The approximation (18) doesn't take into account the contribution of the double-layer boundary integral operator D and avoids an operator inversion. It corresponds to the NtD-choice done in acoustics [6, 4, 5] and electromagnetics [30, 33]. However, the operator D is no more compact in the elasticity case, even for smooths surface. Thus, we also consider its principal part in (19). We will observe in the sequel how it impacts the spectral behavior of the preconditioned CFIE (13). We get the two corresponding P-CFIEs:

- the *High-Order preconditioned CFIE with one term* (HO(1) P-CFIE): integral equation (13) and the analytical preconditioner $\boldsymbol{V}' := \boldsymbol{V}'_{\mathrm{HO}(1)}$ (18) without the contribution $P(D)$ associated with the double-layer boundary integral operator.
- the *High-Order preconditioned CFIE with two terms* (HO(2) P-CFIE): integral equation (13) and the analytical preconditioner $\boldsymbol{V}' := \boldsymbol{V}'_{\mathrm{HO}(2)}$ (19) with the principal part $P(D)$.

The preconditioner $\boldsymbol{V}'$ contains square-root operators of the form $(\Delta_\Gamma + \kappa_\gamma^2 \mathrm{I})^{1/2}$ with $\gamma = s, p$ and their inverse. An artificial singularity of square-root operators appears in the transition zone from the propagating modes to the evanescent ones. The presence of the singularity yields a wrong representation of the grazing modes. To model the behavior in the transition zone, we use a regularization [6] by adding a small local damping parameter $\varepsilon_\gamma > 0$ to the wavenumber κ_γ. We set $\kappa_{\gamma,\varepsilon} := \kappa_\gamma + i\varepsilon_\gamma$ and we consider square-root operators $(\Delta_\Gamma + \kappa_{\gamma,\varepsilon}^2 \mathrm{I})^{1/2}$ and their inverse in the preconditioner $\boldsymbol{V}'$. We denote by $P_\varepsilon(S)$ and $P_\varepsilon(D)$ the corresponding principal parts. The addition of a local damping is important to obtain the well-posed character of the corresponding preconditioned CFIEs. For existence and uniqueness results, we refer to [32].

3.3. Two-dimensional case

The main difference between 2D and 3D for the three proposed preconditioned CFIEs lies in the expressions of the principal parts $P(S)$ and $P(D)$. We denote by s the anticlockwise directed curvilinear abscissa along Γ. We introduce the curvilinear derivative ∂_s. The Laplace-Beltrami operator over Γ is defined by $\Delta_\Gamma := \partial_s^2$. Furthermore, we use the relations $\boldsymbol{\nabla}_\Gamma u = \boldsymbol{\tau}\partial_s u$ and $\mathrm{div}_\Gamma\, \boldsymbol{u} = \partial_s(\boldsymbol{\tau}\cdot\boldsymbol{u})$. We deduce that in 2D we have $P(S) = S_1 + S_2$ with

$$\begin{aligned} S_1 &= \frac{i}{2\rho\omega^2}\Big(\boldsymbol{n}\big(\Delta_\Gamma + \kappa_{p,\varepsilon}^2\mathrm{I}\big)^{\frac{1}{2}}\boldsymbol{n}\cdot\mathrm{I}_{\boldsymbol{n}} + \boldsymbol{\tau}\big(\Delta_\Gamma + \kappa_{s,\varepsilon}^2\mathrm{I}\big)^{\frac{1}{2}}\boldsymbol{\tau}\cdot\mathrm{I}_{\boldsymbol{\tau}}\Big) \\ S_2 &= -\frac{i}{2\rho\omega^2}\Big(\boldsymbol{n}\big(\Delta_\Gamma + \kappa_{s,\varepsilon}^2\mathrm{I}\big)^{-\frac{1}{2}}\Delta_\Gamma(\boldsymbol{n}\cdot\mathrm{I}_{\boldsymbol{n}}) + \boldsymbol{\tau}\big(\Delta_\Gamma + \kappa_{p,\varepsilon}^2\mathrm{I}\big)^{-\frac{1}{2}}\Delta_\Gamma(\boldsymbol{\tau}\cdot\mathrm{I}_{\boldsymbol{\tau}})\Big) \end{aligned} \tag{20}$$

and $P(D) = D_1 + D_2$ with

$$\begin{aligned} D_1 &= \frac{i}{2}\Big(\boldsymbol{n}\partial_s\big(\Delta_\Gamma + \kappa_{p,\varepsilon}^2\mathrm{I}\big)^{-\frac{1}{2}}\boldsymbol{\tau}\cdot\mathrm{I}_{\boldsymbol{\tau}} - \boldsymbol{\tau}\partial_s\big(\Delta_\Gamma + \kappa_{s,\varepsilon}^2\mathrm{I}\big)^{-\frac{1}{2}}\boldsymbol{n}\cdot\mathrm{I}_{\boldsymbol{n}}\Big) \\ D_2 &= \frac{i\mu}{\rho\omega^2}\Big(-\boldsymbol{n}\partial_s\big(\Delta_\Gamma + \kappa_{s,\varepsilon}^2\mathrm{I}\big)^{\frac{1}{2}}\boldsymbol{\tau}\cdot\mathrm{I}_{\boldsymbol{\tau}} + \boldsymbol{n}\partial_s\big(\Delta_\Gamma + \kappa_{p,\varepsilon}^2\mathrm{I}\big)^{-\frac{1}{2}}\Delta_\Gamma(\boldsymbol{\tau}\cdot\mathrm{I}_{\boldsymbol{\tau}}) \\ &\qquad +\boldsymbol{\tau}\partial_s\big(\Delta_\Gamma + \kappa_{p,\varepsilon}^2\mathrm{I}\big)^{\frac{1}{2}}\big(\boldsymbol{n}\cdot\mathrm{I}_{\boldsymbol{n}}\big) - \boldsymbol{\tau}\partial_s\big(\Delta_\Gamma + \kappa_{s,\varepsilon}^2\mathrm{I}\big)^{-\frac{1}{2}}\Delta_\Gamma\big(\boldsymbol{n}\cdot\mathrm{I}_{\boldsymbol{n}}\big)\Big). \end{aligned} \tag{21}$$

4. Spectral study for the spherical case

Once the three possible preconditioned CFIEs presented, we perform an analytical investigation of the eigenvalue clustering of these CFIE operators for the 3D spherical case. We compare also the stability of their condition number with respect to the mesh refinement and frequency increase. We use some results obtained in [32, Section 4 and Appendix B] for the three-dimensional Dirichlet boundary condition case.

4.1. Asymptotic analysis

Let $\mathbf{S}^2$ be the unit sphere in $\mathbb{R}^3$ with outward unit normal vector denoted by $\hat{\boldsymbol{x}}$. We introduce the scalar spherical harmonics $Y_{\ell j}$ of order ℓ for $\ell \in \mathbb{N}$ and degree $j = -\ell, \ldots, \ell$. The concatenation of the tangential vector spherical harmonics defined for $\ell \in \mathbb{N}^*$ by

$$\boldsymbol{\mathcal{Y}}_{\ell j}^{(1)} = (\ell(\ell+1))^{-\frac{1}{2}} \nabla_{\mathbf{S}^2} Y_{\ell j} \ , \quad \boldsymbol{\mathcal{Y}}_{\ell j}^{(1)} = (\ell(\ell+1))^{-\frac{1}{2}} \nabla_{\mathbf{S}^2} Y_{\ell j} \times \hat{\boldsymbol{x}}$$

with the radial spherical harmonics defined for $\ell \in \mathbb{N}$ by $\boldsymbol{\mathcal{Y}}_{\ell j}^{(3)} = \hat{\boldsymbol{x}} Y_{\ell j}$, forms an othonormal basis function of $\boldsymbol{H}^{\frac{1}{2}}(\mathbf{S}^2)$. In the case of an elastic sphere of radius R, the boundary integral operators D and N can be expanded in this basis functions both such that $C\boldsymbol{\mathcal{Y}}_{0,0}^{(3)} = C_0^{(3,3)} \boldsymbol{\mathcal{Y}}_{0,0}^{(3)}$ and for $\ell \geq 1$

$$C \begin{pmatrix} \boldsymbol{\mathcal{Y}}_{\ell,j}^{(1)} \\ \boldsymbol{\mathcal{Y}}_{\ell,j}^{(2)} \\ \boldsymbol{\mathcal{Y}}_{\ell,j}^{(3)} \end{pmatrix} = \begin{pmatrix} C_\ell^{(1,1)} & 0 & C_\ell^{(1,3)} \\ 0 & C_\ell^{(2,2)} & 0 \\ C_\ell^{(3,1)} & 0 & C_\ell^{(3,3)} \end{pmatrix} \begin{pmatrix} \boldsymbol{\mathcal{Y}}_{\ell,j}^{(1)} \\ \boldsymbol{\mathcal{Y}}_{\ell,j}^{(2)} \\ \boldsymbol{\mathcal{Y}}_{\ell,j}^{(3)} \end{pmatrix}$$

where $C = D$ or N. We distinguish three zones of modes: the hyperbolic zone for $\omega R \to +\infty$ and $\ell \ll \kappa_p R$ (propagating modes), the elliptic zone when $\ell \to +\infty$ and $\ell \gg \kappa_s R$ (evanescent modes), and the transition zone of physical surface modes between $\ell \approx \kappa_p R$ and $\ell \approx \kappa_s R$. First, let us consider the hyperbolic zone. We obtain the following asymptotic behavior.

Proposition 4.1. *When $\omega R \to \infty$ we have*

- *for the operator D :*

$$\begin{aligned}
D_\ell^{(1,1)} &= \frac{1}{2} - \sin^2(\kappa_s R - (\ell+1)\tfrac{\pi}{2}) + \tfrac{i}{2}\sin\left(2(\kappa_s R - (\ell+1)\tfrac{\pi}{2})\right) + \mathcal{O}\left(\frac{1}{|\omega R|}\right), \quad \ell \geq 1, \\
D_\ell^{(2,2)} &= \frac{1}{2} - \cos^2(\kappa_s R - (\ell+1)\tfrac{\pi}{2}) - \tfrac{i}{2}\sin\left(2(\kappa_s R - (\ell+1)\tfrac{\pi}{2})\right) + \mathcal{O}\left(\frac{1}{|\omega R|}\right), \quad \ell \geq 1, \\
D_\ell^{(3,3)} &= \frac{1}{2} - \sin^2(\kappa_p R - (\ell+1)\tfrac{\pi}{2}) + \tfrac{i}{2}\sin\left(2(\kappa_p R - (\ell+1)\tfrac{\pi}{2})\right) + \mathcal{O}\left(\frac{1}{|\omega R|}\right), \quad \ell \geq 0, \\
D_\ell^{(1,3)} &= \mathcal{O}\left(\frac{1}{|\omega R|}\right), \quad D_\ell^{(3,1)}(\omega R) = \mathcal{O}\left(\frac{1}{|\omega R|}\right), \quad \ell \geq 1,
\end{aligned}$$

- *and for the operator N :*

$$\begin{aligned}
N_\ell^{(1,1)} &= \frac{\mu\kappa_s}{i}\left(-\cos^2(\kappa_s R - (\ell+1)\tfrac{\pi}{2}) - \tfrac{i}{2}\sin\left(2(\kappa_s R - (\ell+1)\tfrac{\pi}{2})\right)\right) + \mathcal{O}\left(\frac{1}{|\omega R|}\right), \quad \ell \geq 1, \\
N_\ell^{(2,2)} &= \frac{\mu\kappa_s}{i}\left(-\sin^2(\kappa_s R - (\ell+1)\tfrac{\pi}{2}) + \tfrac{i}{2}\sin\left(2(\kappa_s R - (\ell+1)\tfrac{\pi}{2})\right)\right) + \mathcal{O}\left(\frac{1}{|\omega R|}\right), \quad \ell \geq 1, \\
N_\ell^{(3,3)} &= i(\lambda+2\mu)\kappa_p\left(\cos^2(\kappa_p R - (\ell+1)\tfrac{\pi}{2}) + \tfrac{i}{2}\sin\left(2(\kappa_p R - (\ell+1)\tfrac{\pi}{2})\right)\right) + \mathcal{O}\left(\frac{1}{|\omega R|}\right), \ \ell \geq 0, \\
N_\ell^{(1,3)} &= \mathcal{O}\left(\frac{1}{|\omega R|}\right), \quad N_\ell^{(3,1)}(\omega R) = \mathcal{O}\left(\frac{1}{|\omega R|}\right), \quad \ell \geq 1.
\end{aligned}$$

From these results and the integral representation (11), we retrieve the low-order approximation (16) of the NtD operator

$$\boldsymbol{V}'_{\mathrm{LO}} = \begin{pmatrix} \frac{1}{i\mu\kappa_s} & 0 & 0 \\ 0 & \frac{1}{i\mu\kappa_s} & 0 \\ 0 & 0 & \frac{1}{i(\lambda+2\mu)\kappa_p} \end{pmatrix} \tag{22}$$

so that in the hyperbolic zone (when $\omega R \to \infty$) we get

$$\frac{\mathrm{I}}{2} - D + \boldsymbol{V}'_{\mathrm{LO}} N = \mathrm{I} + \mathcal{O}\left(\frac{1}{|\omega R|}\right).$$

The high-order P-CFIE operators share also this good property. Let us observe now the behaviour of the different operators in the elliptic zone. The following asymptotic results hold.

Proposition 4.2. *When $\ell \to \infty$, we have*

- *for the operator D :*

$$\begin{aligned} D_\ell^{(1,1)} &= -\frac{\mu}{\lambda+2\mu}\frac{1}{2(2\ell+1)} + \mathcal{O}\left(\frac{1}{\ell^3}\right), \\ D_\ell^{(2,2)} &= -\frac{3}{2(2\ell+1)} + O\left(\frac{1}{\ell^3}\right), \\ D_\ell^{(3,3)} &= -\frac{3\mu}{\lambda+2\mu}\frac{1}{2(2\ell+1)} + \mathcal{O}\left(\frac{1}{\ell^3}\right), \\ D_\ell^{(1,3)} &= D_\ell^{(3,1)} = \frac{\mu}{2(\lambda+2\mu)} + \mathcal{O}\left(\frac{1}{\ell^2}\right), \end{aligned}$$

- *and for the operator N :*

$$\begin{aligned} N_\ell^{(1,1)} &= \frac{-2\mu(\lambda+\mu)}{\lambda+2\mu}\frac{\ell+\frac{1}{2}}{2R} + \mathcal{O}\left(\frac{1}{\ell}\right), \\ N_\ell^{(2,2)} &= -\mu\frac{\ell+\frac{1}{2}}{2R} + \mathcal{O}\left(\frac{1}{\ell}\right), \\ N_\ell^{(3,3)} &= \frac{-2\mu(\lambda+\mu)}{\lambda+2\mu}\frac{\ell+\frac{1}{2}}{2R} + \mathcal{O}\left(\frac{1}{\ell}\right), \\ N_\ell^{(1,3)} &= N_\ell^{(3,1)} = \frac{\mu(3\lambda+\mu)}{2R(\lambda+2\mu)} + \mathcal{O}\left(\frac{1}{\ell^2}\right). \end{aligned}$$

The asympotic behavior for large modes of the boundary integral operator N are in accordance with the fact that the standard CFIE operator is of the first kind. The application of the low-order approximation $\boldsymbol{V}'_{\mathrm{LO}}$ (22) is not sufficient to regularize the operator N in the elliptic part. It doesn't provide an eigenvalue clustering in this zone (see Figure 1). The high-order approximations are needed to efficiently regularize the operator N. We have

$$\boldsymbol{V}'_{\mathrm{HO}(2)} = -P_\varepsilon(S)\Big(\frac{\mathrm{I}}{2} - P_\varepsilon(D)\Big)^{-1}$$

where

$$P_\varepsilon(S)\begin{pmatrix} \boldsymbol{\mathcal{Y}}_{\ell,j}^{(1)} \\ \boldsymbol{\mathcal{Y}}_{\ell,j}^{(2)} \\ \boldsymbol{\mathcal{Y}}_{\ell,j}^{(3)} \end{pmatrix} = \begin{pmatrix} s_{\ell,\varepsilon}^{(1,1)} & 0 & 0 \\ 0 & s_{\ell,\varepsilon}^{(2,2)} & 0 \\ 0 & 0 & s_{\ell,\varepsilon}^{(3,3)} \end{pmatrix}\begin{pmatrix} \boldsymbol{\mathcal{Y}}_{\ell,j}^{(1)} \\ \boldsymbol{\mathcal{Y}}_{\ell,j}^{(2)} \\ \boldsymbol{\mathcal{Y}}_{\ell,j}^{(3)} \end{pmatrix},$$

with asymptotics when $\ell \to \infty$

$$\begin{aligned}
s_{\ell,\varepsilon}^{(1,1)} &= \frac{i}{2\rho\omega^2}\left[\left(\kappa_{s,\varepsilon}^2 - \frac{\ell(\ell+1)}{R^2}\right)^{\frac{1}{2}} + \frac{\ell(\ell+1)}{R^2}\left(\kappa_{p,\varepsilon}^2 - \frac{\ell(\ell+1)}{R^2}\right)^{-\frac{1}{2}}\right] = \frac{(\kappa_{s,\varepsilon}^2+\kappa_{p,\varepsilon}^2)R}{4\rho\omega^2\sqrt{\ell(\ell+1)}} + o(\ell^{-1}),\\
s_{\ell,\varepsilon}^{(2,2)} &= \frac{i}{2\rho\omega^2}\kappa_{s,\varepsilon}^2\left(\kappa_{s,\varepsilon}^2 - \frac{\ell(\ell+1)}{R^2}\right)^{-\frac{1}{2}} = \frac{\kappa_{s,\varepsilon}^2 R}{2\rho\omega^2\sqrt{\ell(\ell+1)}} + o(\ell^{-1}),\\
s_{\ell,\varepsilon}^{(3,3)} &= \frac{i}{2\rho\omega^2}\left[\left(\kappa_{p}^2 - \frac{\ell(\ell+1)}{R^2}\right)^{\frac{1}{2}} + \frac{\ell(\ell+1)}{R^2}\left(\kappa_{s,\varepsilon}^2 - \frac{\ell(\ell+1)}{R^2}\right)^{-\frac{1}{2}}\right] = \frac{(\kappa_{s,\varepsilon}^2+\kappa_{p,\varepsilon}^2)R}{4\rho\omega^2\sqrt{\ell(\ell+1)}} + o(\ell^{-1}),
\end{aligned}$$

and

$$P_\varepsilon(D)\begin{pmatrix}\boldsymbol{\mathcal{Y}}_{\ell,j}^{(1)}\\ \boldsymbol{\mathcal{Y}}_{\ell,j}^{(2)}\\ \boldsymbol{\mathcal{Y}}_{\ell,j}^{(3)}\end{pmatrix} = \begin{pmatrix}0 & 0 & d_{\ell,\varepsilon}^{(1,3)}\\ 0 & 0 & 0\\ d_{\ell,\varepsilon}^{(3,1)} & 0 & 0\end{pmatrix}\begin{pmatrix}\boldsymbol{\mathcal{Y}}_{\ell,j}^{(1)}\\ \boldsymbol{\mathcal{Y}}_{\ell,j}^{(2)}\\ \boldsymbol{\mathcal{Y}}_{\ell,j}^{(3)}\end{pmatrix},$$

with asymptotics when $\ell \to \infty$

$$\begin{aligned}
d_{\ell,\varepsilon}^{(1,3)} &= \frac{i}{\kappa_{s,\varepsilon}^2}\left(\frac{\ell(\ell+1)}{R^2}\right)^{1/2}\left[\left(\kappa_{s,\varepsilon}^2 - \frac{\ell(\ell+1)}{R^2}\right)^{\frac{1}{2}} + \frac{\ell(\ell+1)}{R^2}\left(\kappa_{p,\varepsilon}^2 - \frac{\ell(\ell+1)}{R^2}\right)^{-\frac{1}{2}}\right]\\
&\quad -\frac{i}{2}\left(\frac{\ell(\ell+1)}{R^2}\right)^{1/2}\left(\kappa_{p,\varepsilon}^2 - \frac{\ell(\ell+1)}{R^2}\right)^{-\frac{1}{2}} = \frac{\kappa_{p,\varepsilon}^2}{2\kappa_{s,\varepsilon}^2} + o(1),\\
d_{\ell,\varepsilon}^{(3,1)} &= \frac{i}{\kappa_{s,\varepsilon}^2}\left(\frac{\ell(\ell+1)}{R^2}\right)^{1/2}\left[\left(\kappa_{p,\varepsilon}^2 - \frac{\ell(\ell+1)}{R^2}\right)^{\frac{1}{2}} + \frac{\ell(\ell+1)}{R^2}\left(\kappa_{s,\varepsilon}^2 - \frac{\ell(\ell+1)}{R^2}\right)^{-\frac{1}{2}}\right]\\
&\quad -\frac{i}{2}\left(\frac{\ell(\ell+1)}{R^2}\right)^{1/2}\left(\kappa_{s,\varepsilon}^2 - \frac{\ell(\ell+1)}{R^2}\right)^{-\frac{1}{2}} = \frac{\kappa_{p,\varepsilon}^2}{2\kappa_{s,\varepsilon}^2} + o(1).
\end{aligned}$$

Thus, we obtain the following behaviour of the high-order approximate NtD map when $\ell \to \infty$

$$\boldsymbol{V}'_{\mathrm{HO}(2)}\begin{pmatrix}\boldsymbol{\mathcal{Y}}_{\ell,j}^{(1)}\\ \boldsymbol{\mathcal{Y}}_{\ell,j}^{(2)}\\ \boldsymbol{\mathcal{Y}}_{\ell,j}^{(3)}\end{pmatrix} = -\frac{R}{\sqrt{\ell(\ell+1)}}\begin{pmatrix}\frac{1}{2\rho\omega^2}\frac{\kappa_{s,\varepsilon}^4}{\kappa_{s,\varepsilon}^2-\kappa_{p,\varepsilon}^2} & 0 & \frac{1}{2\rho\omega^2}\frac{\kappa_{s,\varepsilon}^2\kappa_{p,\varepsilon}^2}{\kappa_{s,\varepsilon}^2-\kappa_{p,\varepsilon}^2}\\ 0 & \frac{\kappa_{s,\varepsilon}^2}{\rho\omega^2} & 0\\ \frac{1}{2\rho\omega^2}\frac{\kappa_{s,\varepsilon}^2\kappa_{p,\varepsilon}^2}{\kappa_{s,\varepsilon}^2-\kappa_{p,\varepsilon}^2} & 0 & \frac{1}{2\rho\omega^2}\frac{\kappa_{s,\varepsilon}^4}{\kappa_{s,\varepsilon}^2-\kappa_{p,\varepsilon}^2}\end{pmatrix}\begin{pmatrix}\boldsymbol{\mathcal{Y}}_{\ell,j}^{(1)}\\ \boldsymbol{\mathcal{Y}}_{\ell,j}^{(2)}\\ \boldsymbol{\mathcal{Y}}_{\ell,j}^{(3)}\end{pmatrix} + o(\ell^{-1})$$

and of the corresponding HO(2) P-CFIE operator

$$\begin{aligned}
&\left(\frac{\mathrm{I}}{2} - D + \boldsymbol{V}'_{\mathrm{HO}(2)}N\right)\begin{pmatrix}\boldsymbol{\mathcal{Y}}_{\ell,j}^{(1)}\\ \boldsymbol{\mathcal{Y}}_{\ell,j}^{(2)}\\ \boldsymbol{\mathcal{Y}}_{\ell,j}^{(3)}\end{pmatrix}\\
&= \begin{pmatrix}\frac{1}{2} + \frac{\kappa_{s,\varepsilon}^4(\kappa_s^2-\kappa_p^2)}{2\kappa_s^4(\kappa_{s,\varepsilon}^2-\kappa_{p,\varepsilon}^2)} & & \frac{\mu}{2(\lambda+2\mu)}\left(\frac{\kappa_{s,\varepsilon}^2\kappa_{p,\varepsilon}^2(\kappa_s^2-\kappa_p^2)}{\kappa_s^2\kappa_p^2(\kappa_{s,\varepsilon}^2-\kappa_{p,\varepsilon}^2)} - 1\right)\\ 0 & \frac{1}{2} + \frac{\kappa_{s,\varepsilon}^2}{2\kappa_s^2} & 0\\ \frac{\mu}{2(\lambda+2\mu)}\left(\frac{\kappa_{s,\varepsilon}^2\kappa_{p,\varepsilon}^2(\kappa_s^2-\kappa_p^2)}{\kappa_s^2\kappa_p^2(\kappa_{s,\varepsilon}^2-\kappa_{p,\varepsilon}^2)} - 1\right) & 0 & \frac{1}{2} + \frac{\kappa_{s,\varepsilon}^4(\kappa_s^2-\kappa_p^2)}{2\kappa_s^4(\kappa_{s,\varepsilon}^2-\kappa_{p,\varepsilon}^2)}\end{pmatrix}\begin{pmatrix}\boldsymbol{\mathcal{Y}}_{\ell,j}^{(1)}\\ \boldsymbol{\mathcal{Y}}_{\ell,j}^{(2)}\\ \boldsymbol{\mathcal{Y}}_{\ell,j}^{(3)}\end{pmatrix} + o(\ell^{-1}).
\end{aligned}$$

This result shows that the eigenvalues of the HO(2)-CFIE operator are well-clustered around the unit in the elliptic zone. This is also the case for the HO(1)-CFIE operator.

4.2. Illustration of the spectral properties for the unit sphere

We now consider a finite dimensional approximation. We keep only the modes ℓ such that $|\ell| \leq m_{\max}$ with $m_{\max} = [(n_{\lambda_s}\kappa_s R)/2]$ and $[x]$ denotes the integer part of a real number x. In practice, the number of modes $m_{\max}$ to retain must not only be large enough to capture the hyperbolic and transition parts of the spectrum but also the elliptic part ($m_{\max} \geq \kappa_s$), while

avoiding the divergence of the spherical Bessel and Hankel functions. It depends on the density of discretization points n_{λ_s} per S-wavelength ($\lambda_s = 2\pi/\kappa_s$).

In this Section, the physical parameters ($\rho = \mu = 1$, $\lambda = 3$) are fixed such that the wavenumbers satisfy $\kappa_s = \sqrt{5}\kappa_p$. In Figure 1, we report the eigenvalue distribution of the standard and three proposed P-CFIEs. We observe that the three analytical preconditioners improve successfully the spectral properties of the standard CFIE with an efficient clustering of the eigenvalues. The best results are given by the HO P-CFIEs, particularly in the elliptic zone. As expected, the corresponding condition numbers are independent on the number of modes, i.e. on the mesh density (see Figure 2), on the contrary to the standard CFIE of the first-kind. Furthermore, the LO and HO P-CFIEs allow to reduce the dependance of the condition number with respect to the frequency. This dependance is linked to the eigenvalues associated with grazing modes. We have performed also this analytical study for the unit disk in 2D and obtain similar conclusions (see Figure 3).

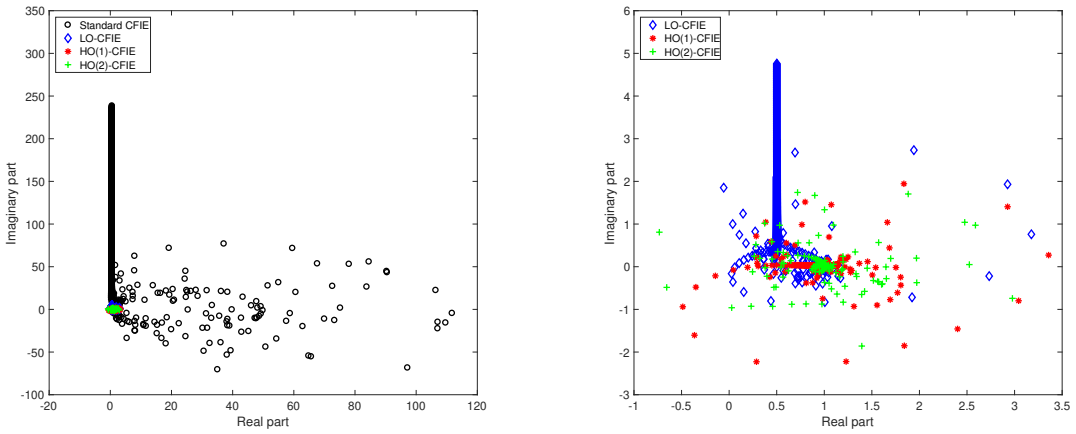

(a) (b)

Figure 1: Unit sphere. Distribution of the eigenvalues of the standard and three P-CFIEs ($\eta = 1$, $\kappa_s = \omega = 50$ and $n_{\lambda_s} = 12$). (a) Complete distribution and (b) Closer view on the clustering.

5. Numerical efficiency of analytical preconditioners

5.1. Discretization and implementation

To discretize the surface Γ of the scatterer, we consider a triangulation with N_E surface triangles and N_I vertices. The polyedric interpolated surface is denoted by Γ_h. The discretization is performed by means of classical $\mathbb{P}_1$ boundary finite elements. We set $X_h = \mathbb{P}_1(\Gamma_h)$ and $\boldsymbol{X}_h = V_h^d$, $d = 2, 3$, with $\dim \boldsymbol{X}_h = M := dN_I$. The application of the HO(2)-preconditioner (19), namely

$$\boldsymbol{V}'_{\mathrm{HO(2)}} = -P_\varepsilon(S)\Big(\frac{\mathrm{I}}{2} - P_\varepsilon(D)\Big)^{-1},$$

is decomposed into the following two steps:

Step 1: Knowing $\boldsymbol{v} \in \boldsymbol{H}^{\frac{1}{2}}(\Gamma)$, solve the boundary differential equation: find the intermediate variable $\boldsymbol{q} \in \boldsymbol{H}^{\frac{1}{2}}(\Gamma)$ solution of

$$\Big(\frac{\mathrm{I}}{2} - P_\varepsilon(D)\Big)\boldsymbol{q} = \boldsymbol{v}. \tag{23}$$

Step 2: Knowing $\boldsymbol{q} \in \boldsymbol{H}^{\frac{1}{2}}(\Gamma)$, compute $\boldsymbol{u} \in \boldsymbol{H}^{-\frac{1}{2}}(\Gamma)$ such that

$$\boldsymbol{u} = -P_\varepsilon(S)\boldsymbol{q}. \tag{24}$$

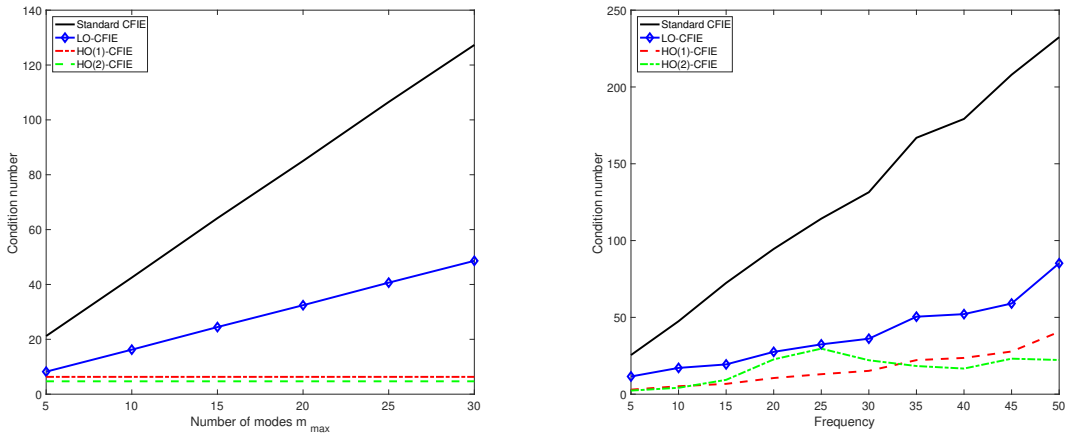

(a) (b)

Figure 2: Unit sphere. Study of the condition number of the three P-CFIEs. (a) Condition number with respect to the maximal number of modes $m_{\max}$ ($\kappa_s = 4\pi$). (b) Condition number with respect to the frequency ω ($n_{\lambda_s} = 12$).

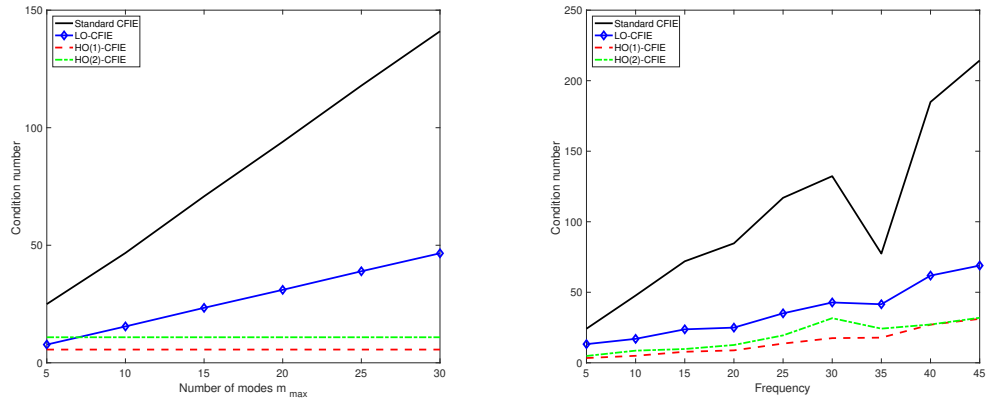

(a) (b)

Figure 3: Unit disk. Study of the condition number of the P-CFIEs. (a) Condition number with respect to the maximal number of modes $m_{\max}$ ($\kappa_s = 4\pi$). (b) Condition number with respect to the frequency ($n_{\lambda_s} = 12$).

The application of the HO(1)-preconditioner (18), i.e. without the contribution of the operator D, reduces to the evaluation of $\boldsymbol{u} = -2P_\varepsilon(S)\boldsymbol{v}$ without the need of the inversion Step (**Step 1**). We refer to [21] for the derivation of the corresponding variational formulation. The efficiency of the HO-preconditioners relies on a robust local representation of the square-root operators $(1+z)^{1/2}$, $z \in \mathbb{C}$, and their inverses. To this end, we apply complex Padé approximants with a rotating branch-cut of angle θ (see [52, 22] for more details). Such a Padé approximation allows to model correctly the different types of modes and in particular the evanescent ones, i.e. corresponding to the region $\{z < -1 | \mathrm{Im}(z) = 0\}$. The discrete wavenumbers are then expressed by $\kappa_{\gamma,\varepsilon_h} = \kappa_s + i\varepsilon_h$ with $\varepsilon_h = 0.39\kappa_\gamma^{1/3}(\mathcal{H}_h^2)^{1/3}$. The quantity $\mathcal{H}_h$ is a piecewise constant interpolation of the mean curvature $\mathcal{H}$ over Γ_h on each triangle of the triangulation. The numerical evaluation of $\mathcal{H}_h$ comes

from the relation

$$\mathcal{H}_h(\boldsymbol{x}) = \frac{1}{2}\,\mathrm{div}_{\Gamma_h}\,\boldsymbol{n}_h(\boldsymbol{x}) = \frac{1}{2}\sum_{k=1}^{d}\sum_{j=1}^{N_I}(\boldsymbol{n}_h(\boldsymbol{a}_j)\cdot\boldsymbol{e}_k)(\boldsymbol{e}_k\cdot\nabla_{\Gamma_h}\varphi_j(\boldsymbol{x})), \quad \boldsymbol{x}\in\Gamma_h,$$

where $\boldsymbol{a}_j$, $1\le j\le N_I$, are the vertices of the mesh and the functions φ_j, $1\le j\le N_I$, the $\mathbb{P}_1$ basis functions on Γ_h.

We solve the dense non-symmetric linear systems, corresponding to the BEM discretization of the preconditioned or standard CFIEs, with GMRES [60]. We do not use a restarted version in order to have a precise idea of the impact of the preconditioning technique on the convergence. $[A]\in\mathbb{C}^{M\times M}$ denotes the matrix associated with the linear discretization of a given integral operator A. At each iteration of the solver, the solution of the preconditioned CFIE (13) requires the evaluation of the vector $\mathbf{Y}\in\mathbb{C}^M$

$$\mathbf{Y} = \left(\frac{[\mathrm{I}]}{2} + [D] + [\boldsymbol{V}'][N]\right)\mathbf{X},$$

for any vector $\mathbf{X}\in\mathbb{C}^M$ given by GMRES. From a computational point of view, the preconditioners (18) and (19) involve only sparse matrices. The Padé approximation of order $2N_p+1$ requires to solve N_p uncoupled sparse linear systems. Importantly, for the preconditioner (19) **Step 1** needs the inversion of $\Big(\mathrm{I}/2 - P_\varepsilon(D))\Big)$. In practice, due to the use of Padé approximations, the matrix associated with this operator is never explicitly assembled and the sparse system is solved with an inner GMRES solver.

To check the efficiency of the proposed analytical preconditioners, we consider three geometries with increasing difficulties. The first geometry is a unit disk used to validate our code. The second one is a unit square with corner singularities. Finally, we construct a C-shape modeling a crack with a finite thickness (see Fig. 4). It is parametrised by $\mathcal{C} = \{(1.5\sin\frac{(3t+4)\pi}{8} - 1, 0.8\sin\frac{(3t+4)\pi}{4}) : -1\le t\le 1\}\cup\{(1.45\sin\frac{(3t+4)\pi}{8} - 1, 0.7\sin\frac{(3t+4)\pi}{4}) :\ -1\le t\le 1\}$. For all the examples, we fix the mechanical parameters to $\rho=\mu=1$ and $\lambda=2$ such that $\kappa_s=\omega$ and $\kappa_p=\omega/2$. The obstacles are meshed with a density of n_{λ_s} points per S-wavelength.

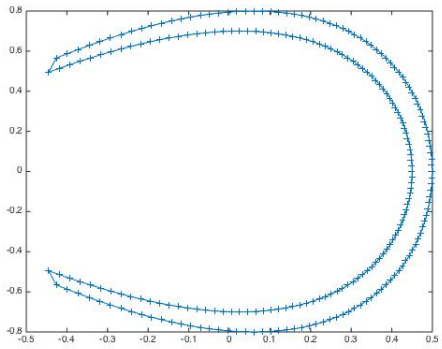

Figure 4: C-shape: definition of the geometry.

5.2. Spectral analysis

In order to analyse the convergence properties of GMRES to solve the preconditioned and standard CFIEs, we observe first the eigenvalue behavior of the involved integral operators. The spectral study has been done analytically for the unit disk in Section 4. For the unit square and the C-shape, an analytical expression of the eigenvalues is not available. We compute them

numerically to check if these good spectral properties are also observed. The circular frequency is set to $\omega = 2\pi$, the discretization to $n_{\lambda_s} = 20$ and the Padé order to 60. We report on Figures 5 and 6 the eigenvalue distribution for the standard and preconditioned CFIEs when the scatterers are the unit square and the C-shape respectively. For these scatterers, the high order local approximation of the NtD maps also have the remarkable property of clustering the eigenvalues associated with the evanescent modes. This is not the case for the non-preconditioned CFIE. The best spectral behavior is provided by the HO(2)-preconditioner and is favorable for an iterative solution.

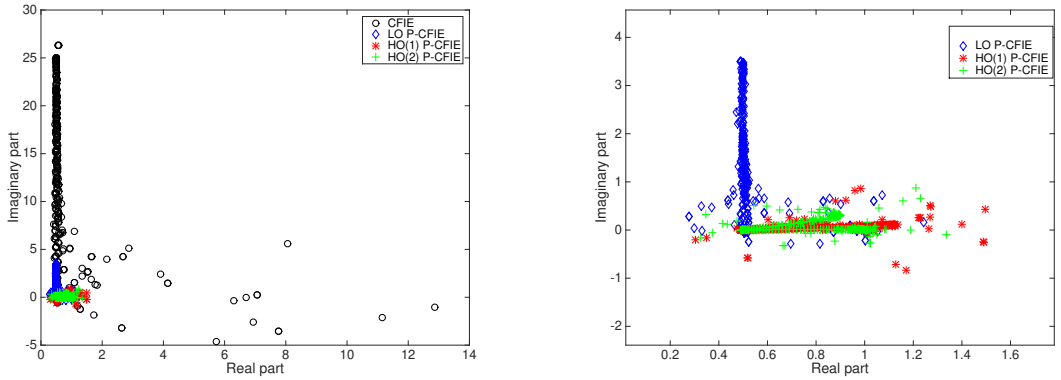

(a) (b)

Figure 5: Unit square. Distribution of the eigenvalues of the standard and different P-CFIEs ($\eta = 1$, $\omega = 2\pi$ and $n_{\lambda_s} = 20$). (a) Complete distribution and (b) closer view of the clustering.

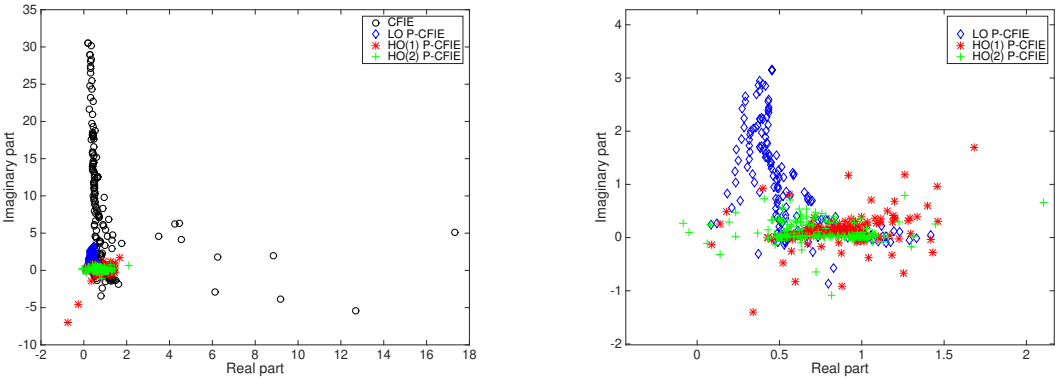

(a) (b)

Figure 6: C-shape. Distribution of the eigenvalues of the standard and different P-CFIEs ($\eta = 1$, $\omega = 2\pi$ and $n_{\lambda_s} = 20$). (a) Complete distribution and (b) closer view of the clustering.

5.3. Numerical efficiency in the context of an iterative solver

We now compare the convergence of the iterative solver GMRES for the different CFIEs. The scatterers are illuminated by incident plane waves of the form

$$\boldsymbol{u}^{\text{inc}}(\boldsymbol{x}) = \frac{1}{\mu}\, e^{i\kappa_s \boldsymbol{x}\cdot\boldsymbol{d}}(\boldsymbol{d}\times\boldsymbol{p})\times\boldsymbol{d} + \frac{1}{\lambda+2\mu}\, e^{i\kappa_p \boldsymbol{x}\cdot\boldsymbol{d}}(\boldsymbol{d}\cdot\boldsymbol{p})\boldsymbol{d}, \quad \text{where } \boldsymbol{d}\in\mathbf{D}^2 \text{ and } \boldsymbol{p}\in\mathbb{R}^2 \tag{25}$$

($\mathbf{D}^2$ is the unit disk in $\mathbb{R}^2$). When $\boldsymbol{p} = \pm\boldsymbol{d}$, the incident plane wave oscillates along the direction of propagation (pressure wave or P-wave). When the polarization $\boldsymbol{p}$ is orthogonal to the propagation

vector $\boldsymbol{d}$, the incident plane wave oscillates in a direction orthogonal to the direction of propagation (shear wave or S-wave). We consider the scattering of incident plane P-waves with $\boldsymbol{p} = \boldsymbol{d} = (1,0)^T$, or S-waves with $\boldsymbol{p} = (1,0)^T$ and $\boldsymbol{d} = (0,1)^T$. For all the tests, the tolerances of the inner and outer GMRES solvers are set to 10^{-5} and 10^{-3} respectively. The mechanical parameters are defined such that the wavenumbers satisfy $\kappa_s = 2\kappa_p$ and $\omega = \kappa_s$ (i.e. $\rho = 1$, $\mu = 1$ and $\lambda = 2$) and the number of Padé terms is set to 60.

Unit disk. As a usual validation test, we first consider the unit disk. Figure 7 represents the analytical and numerical far fields for $n_{\lambda_s} = 40$ and $\omega = 2\pi$ and illustrates the accuracy of the code (for an incident plane P wave). The number of GMRES iterations with respect to the frequency ω are reported in Table 1 (resp. Table 2) for P-waves (resp. S-waves) for the four possible CFIEs. In the case of the HO(2) P-CFIE, inner iterations are indicated in parentheses. The use of the different analytical preconditioners efficiently speeds up the convergence of the solver, particularly at high frequencies. The HO(2) P-CFIE provides the best results. Nevertheless, the two other P-CFIEs also offer a very good alternative to the standard CFIE and have the advantage to be very simple to implement. The dependence of the convergence with respect to the frequency is linked to eigenvalues corresponding with grazing modes and probably surface modes (Rayleigh waves). In Table 3, we study the number of GMRES iterations with respect to the density of points n_{λ_s} for incident S-waves. As predicted by the spectral analysis, the convergence is independent on the mesh refinement for the HO P-CFIEs. The LO P-CFIE is also robust with a slight increase of the number of iterations. This is not the case of the standard CFIE which is of the first-kind.

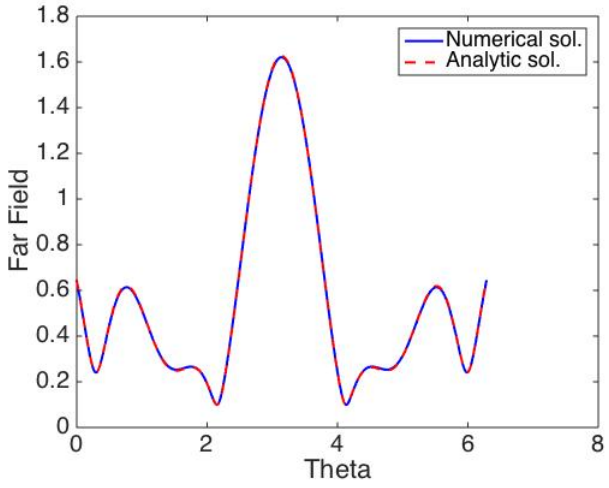

Figure 7: Unit disk. Validation of the code by comparing the analytical and numerical modulus of the far-field for an incident plane P-wave ($n_{\lambda_s} = 40$ and $\omega = 2\pi$). The L^2 error for this example is 5.87 10^{-3}.

ω	# iter CFIE	# iter LO P-CFIE	# iter HO(1) P-CFIE	# iter HO(2) P-CFIE
2π	20	6	8	5(22)
4π	32	9	11	4(30)
6π	50	12	11	4(32)
8π	72	13	12	3(33)
16π	120	11	8	3(40)
20π	170	10	8	3(45)

Table 1: Unit disk: Diffraction of incident P-waves. Number of GMRES iterations for a fixed density of points $n_{\lambda_s} = 20$.

ω	# iter CFIE	# iter LO P-CFIE	# iter HO(1) P-CFIE	# iter HO(2) P-CFIE
2π	26	13	11	8(24)
4π	46	19	19	8(32)
6π	65	27	25	9(39)
8π	91	36	31	10(45)
16π	186	66	51	14(68)

Table 2: Unit disk: Diffraction of incident S-waves. Number of GMRES iterations for a fixed density of points $n_{\lambda_s} = 20$.

n_{λ_s}	# iter CFIE	# iter LO P-CFIE	# iter HO(1) P-CFIE	# iter HO(2) P-CFIE
5	31	14	19	9(30)
10	37	16	17	6(33)
20	46	19	19	8(32)
30	57	22	19	8(32)

Table 3: Unit disk. Diffraction of incident S-waves. Number of GMRES iterations for a fixed frequency $\omega = 4\pi$.

Unit square. We now consider the case of a unit square. The number of GMRES iterations with respect to the frequency ω are reported in Table 4 (resp. Table 5) for P-waves (resp. S-waves) for the four possible CFIEs. In Table 6, we study the number of GMRES iterations with respect to the density of points n_{λ_s} for incident S-waves. For this geometry more difficult geometry, the number of iterations without any preconditioner also increases with both the frequency and the mesh refinement. The three preconditioners are efficient. Here again, the dependence on the frequency after preconditioning is reduced, and the independence of the convergence according to a mesh refinement is still observed with the HO P-CFIEs.

ω	# iter CFIE	# iter LO P-CFIE	# iter HO(1) P-CFIE	# iter HO(2) P-CFIE
2π	57	19	11	10(25)
4π	103	25	15	11(35)
6π	134	30	21	13(42)
8π	177	36	28	15(52)
16π	287	55	49	20(80)

Table 4: Unit square. Diffraction of incident P-waves. Number of GMRES iterations for a fixed density of points $n_{\lambda_s} = 20$.

ω	# iter CFIE	# iter LO P-CFIE	# iter HO(1) P-CFIE	# iter HO(2) P-CFIE
2π	63	21	12	10(25)
4π	120	26	18	12(35)
6π	171	32	23	15(43)
8π	226	38	29	17(52)
16π	421	70	53	24(80)

Table 5: Unit square. Diffraction of incident S-waves. Number of GMRES iterations for a fixed density of points $n_{\lambda_s} = 20$.

n_{λ_s}	# iter CFIE	# iter LO P-CFIE	# iter HO(1) P-CFIE	# iter HO(2) P-CFIE
20	421	70	53	24(80)
30	449	86	55	23(80)
40	475	99	55	24(80)

Table 6: Unit square. Diffraction of incident S-waves. Number of GMRES iterations for a fixed frequency $\omega = 16\pi$.

C-shape. It is known that the dependence on the frequency is more pronounced for the case of a trapping obstacle than for the case of a disk or square. It is interesting to study the efficiency of analytical preconditioners for such scattering objects. The number of GMRES iterations with respect to the frequency ω are reported in Table 7 (resp. Table 8) for P-waves (resp. S-waves) for the four possible CFIEs. For this more difficult geometry, the number of iterations without any preconditioner increases drastically with the frequency. The three preconditioners are seen to be very efficient (with at least the number of iterations divided by three). Here again, the dependence on the frequency after preconditioning is reduced. Importantly, for this geometry HO(1) P-CFIE is the most robust approach particularly at high frequencies. For example, where multiplying the frequency by 8, the number of iterations is only multiplied by a factor 2. The relative loss of performance of the HO(2) P-CFIE approach for this geometry can be explained by the inversion of the operator $\left(\frac{\mathrm{I}}{2} - P_\varepsilon(D)\right)$ in (23), where $P_\varepsilon(D)$ is the principal part of the non-compact operator D. For Dirichlet problems, we proposed to consider a modified potential theory (using the tangential Günter derivative) in which the corresponding double-layer boundary integral operator is a compact operator [32, 31]. This technique is not possible for Neumann problems. The inversion in (23) requires a higher Padé order to make the HO(2) P-CFIE competitive. The HO(1) P-CFIE is a very interesting compromise for such configurations.

ω	# iter CFIE	# iter LO P-CFIE	# iter HO(1) P-CFIE	# iter HO(2) P-CFIE
2π	66	27	25	28(40)
4π	106	34	31	46(54)
6π	176	47	45	66(73)
8π	207	44	41	79(84)
16π	332	61	52	113(141)

Table 7: C-shape: Diffraction of incident P-wave. Number of GMRES iterations for a fixed density of points $n_{\lambda_s} = 20$.

ω	N	# iter CFIE	# iter LO P-CFIE	# iter HO(1) P-CFIE	# iter HO(2) P-CFIE
2π	81	65	26	25	28(40)
4π	165	122	35	31	46(54)
6π	250	180	47	46	68(72)
8π	331	205	51	41	75(83)
16π	666	328	69	56	107(140)
20π	829	395	76	61	116(173)

Table 8: C-shape: Diffraction of incident S-wave. Number of GMRES iterations for a fixed density of points $n_{\lambda_s} = 20$.

6. Conclusion and future work

In this paper, we have presented a first conclusive study of the efficiency of analytical preconditioners for the numerical solution of high-oscillatory Neumann elastic exterior problems. We

have proposed three preconditioners corresponding to approximations with various orders of the exact adjoint Neumann-to-Dirichlet (NtD) map. The theory based on the calculus of the principal pseudo-differential symbol of the NtD map is described in two- and three-dimensions.

A spectral analytical study for the spherical case has shown that the high-order preconditioned CFIEs are not of the first-kind on the contrary to the non-preconditioned CFIE. Consequently, their condition numbers are not sensitive to the mesh refinement and the convergence of GMRES is independent of the mesh size too. Numerical simulations on various 2D geometries have attested that the convergence of GMRES is also greatly improved with respect to the frequency with high-order and local approximations of the NtD. A slight dependence on the frequency is observed. Nevertheless, the proposed preconditioned CFIEs offer a very competitive alternative to the standard one.

In the future, a more extensive analysis should be performed in order to understand the influence in the preconditioner of some physical aspects inherent to a cavity problem, e.g. surface Rayleigh waves. This is an ongoing work.

[1] F. Alouges, S. Borel, and D. P. Levadoux, *A stable well-conditioned integral equation for electromagnetism scattering*, J. Comput. Appl. Math., 204 (2007), pp. 440–451.

[2] X. Antoine, H. Barucq, and A. Bendali, *Bayliss-turkel-like radiation condition on surfaces of arbitrary shape*, J. Math. Anal. Appl., 229 (1999), pp. 184–211.

[3] X. Antoine, A. Bendali, and M. Darbas., *Analytic preconditioners for the boundary integral solution of the scattering of acoustic waves by open surfaces*, Journal of Computational Acoustics, 13 (2005), pp. 477–498.

[4] X. Antoine and M. Darbas, *Alternative integral equations for the iterative solution of acoustic scattering problems*, Quart. J. Mech. Appl. Math., 58 (2005), pp. 107–128.

[5] X. Antoine and M. Darbas, *Generalized combined field integral equations for the iterative solution of the three-dimensional Helmholtz equation*, M2AN Math. Model. Numer. Anal., 41 (2007), pp. 147–167.

[6] X. Antoine, M. Darbas, and Y. Y. Lu, *An improved surface radiation condition for high-frequency acoustic scattering problems*, Comput. Methods Appl. Mech. Engrg., 195 (2006), pp. 4060–4074.

[7] M. Bebendorf and R. Grzhibovskis, *Accelerating galerkin bem for linear elasticity using adaptive cross approximation*, Math. Methods Appl. Sci., 29 (2006), pp. 1721–1747.

[8] J. P. Berenger, *A perfectly matched layer for the absorption of electromagnetic waves*, Journal of computational physics, 114 (1994), pp. 185–200.

[9] J. Bielak, K. Loukakis, Y. Hisada, and C. Yoshimura, *Domain reduction method for three-dimensional earthquake modeling in localized regions, part i: Theory*, Bulletin of the Seismological Society of America, 93 (2003), pp. 817–824.

[10] M. Bonnet, *Boundary integral equations methods in solids and fluids*, John Wiley and sons, 1999.

[11] Y. Boubendir and C. Turc, *Well-conditioned boundary integral equation formulations for the solution of high-frequency electromagnetic scattering problems*, Computers and Mathematics with Applications, 67 (2014), pp. 1772–1805.

[12] O. Bruno, T. Elling, R. Paffenroth, and C. Turc, *Electromagnetic integral equations requiring small numbers of krylov-subspace iterations*, Journal of Computational Physics, 228 (2009), pp. 6169–6183.

[13] O. Bruno, T. Elling, and C. Turc, *Regularized integral equations and fast high-order solvers for sound-hard acoustic scattering problems*, International Journal for Numerical Methods in Engineering, 91 (2012), pp. 1045–1072.

[14] O. Bruno and S. Lintner, *Second-kind integral solvers for TE and TM problems of diffraction by open arcs*, Radio Science, 47 (2012).

[15] B. Carpentieri, *A matrix-free two-grid preconditioner for solving boundary integral equations in electromagnetism*, Computing, 77 (2006), pp. 275–296.

[16] B. Carpentieri, I. Duff, and L. Giraud, *Some sparse pattern selection strategies for robust frobenius norm minimization preconditioners in electromagnetism*, Numer. Linear Algebra Appl., 7 (2000), pp. 667–685.

[17] B. Carpentieri, I. S. Duff, L. Giraud, and G. Sylvand, *Combining fast multipole techniques and an approximate inverse preconditioner for large parallel electromagnetics calculations*, SIAM J. Sci. Comp., 27 (2005), pp. 774–792.

[18] C. Cerjan, D. Kosloff, R. Kosloff, and M. Reshef, *A nonreflecting boundary condition for discrete acoustic and elastic wave equations*, Geophysics, 50 (1985), pp. 705–708.

[19] S. Chaillat and M. Bonnet, *Recent advances on the fast multipole accelerated boundary element method for 3D time-harmonic elastodynamics*, Wave Motion, 50 (2013), pp. 1090–1104.

[20] S. Chaillat, M. Bonnet, and J. F. Semblat, *A multi-level fast multipole BEM for 3-D elastodynamics in the frequency domain*, Comput. Methods Appl. Mech. Engng., 197 (2008), pp. 4233–4249.

[21] S. Chaillat, M. Darbas, and F. Le Louër, *Approximate local dirichlet-to-neumann map for three-dimensional time-harmonic elastic waves*, Computer Methods in Applied Mechanics and Engineering, 297 (2015), pp. 62–83.

[22] ———, *Fast iterative boundary element methods for high-frequency scattering problems in 3d elastodynamics*, Journal of Computational Physics, 341 (2017), pp. 429–446.

[23] S. Chaillat, J. F. Semblat, and M. Bonnet, *A preconditioned 3-d multi-region fast multipole solver for seismic wave propagation in complex geometries.*, Commun. Comp. Phys., 11 (2012), pp. 594–609.

[24] E. Chaljub, D. Komatitsch, J.-P. Vilotte, Y. Capdeville, B. Valette, and G. Festa, *Spectral-element analysis in seismology*, Advances in Geophysics, 48 (2007), pp. 365–419.

[25] S. Chandler-Wilde, I. G. Graham, S. Langdon, and E. A. Spence, *Numerical-asymptotic boundary integral methods in high-frequency acoustic scattering*, Acta Numerica, 21 (2012), pp. 89–305.

[26] W. C. Chew and Q. H. Liu, *Perfectly matched layers for elastodynamics: a new absorbing boundary condition*, Journal of Computational Acoustics, 4 (1996), pp. 341–359.

[27] S. Christiansen, *Discrete fredholm properties and convergence estimates for the electric field integral equation*, Math. Comp., 73 (2004), pp. 143–167.

[28] S. Christiansen and J. C. Nédélec, *A preconditioner for the electric field integral equation based on calderon formulas*, SIAM J. Numer. Anal., 40 (2002), pp. 1100–1135.

[29] R. Clayton and B. Engquist, *Absorbing boundary conditions for acoustic and elastic wave equations*, Bulletin of the Seismological Society of America, 67 (1977), pp. 1529–1540.

[30] M. Darbas, *Generalized combined field integral equations for the iterative solution of the three-dimensional Maxwell equations*, Appl. Math. Lett., 19 (2006), pp. 834–839.

[31] M. Darbas, E. Darrigrand, and Y. Lafranche, *Combining OSRC preconditioning and Fast Multipole Method for the Helmholtz equation*, J. Comput. Phys., 236 (2013), pp. 289–316.

[32] M. Darbas and F. Le Louër, *Well-conditioned boundary integral formulations for the iterative solution of elastic scattering problems*, Mathematical Methods in the Applied Sciences, 38 (2015), pp. 1705–1733.

[33] M. El Bouajaji, X. Antoine, and C. Geuzaine, *Approximate local magnetic-to-electric surface operators for time-harmonic maxwell's equations*, Journal of Computational Physics, 279 (2014), pp. 241–260.

[34] B. Engquist and A. Majda, *Radiation boundary conditions for acoustic and elastic wave calculations*, Comm. Pure Appl. Math., 32 (1979), pp. 314–358.

[35] P. Escapil-Inchauspé and C. Jerez-Hanckes, *Fast calderón preconditioning for the electric field integral equation*, IEEE Transactions on Antennas and Propagation, 67 (2019), pp. 2555–2564.

[36] I. Fierro and C. Jerez-Hanckes, *Fast calderón preconditioning for helmholtz boundary integral equations*, Journal of Computational Physics, (2020), p. 109355.

[37] G. K. Gächter and M. J. Grote, *Dirichlet-to-Neumann map for three-dimensional elastic waves*, Wave Motion, 37 (2003), pp. 293–311.

[38] D. Givoli, *High-order nonreflecting boundary conditions without high-order derivatives*, Journal of Computational Physics, 122 (2001), pp. 849–870.

[39] R. W. Graves, *Simulating seismic wave propagation in 3D elastic media using staggered-grid finite differences*, Bulletin of the Seismological Society of America, 86 (1996), pp. 1091–1106.

[40] L. Halpern, S. Petit-Bergez, and J. Rauch, *The analysis of matched layers*, Confluentes Mathematici, 3 (2011), pp. 159–236.

[41] J. S. Hesthaven and T. Warburton, *Nodal discontinuous Galerkin methods: algorithms, analysis, and applications*, vol. 54, Springer, 2007.

[42] G. C. Hsiao and W. L. Wendland, *Boundary integral equations*, vol. 164 of Applied Mathematical Sciences, Springer-Verlag, Berlin, 2008.

[43] D. S. Jones, *An approximate boundary condition in acoustics*, J. Sound Vibr., 121 (1998), pp. 37–45.

[44] D. Komatitsch and J. P. Vilotte, *The spectral element method: an efficient tool to simulate the seismic response of 2D and 3D geological structures*, Bulletin of the seismological society of America, 88 (1998), pp. 368–392.

[45] R. Kress, *Minimizing the condition number of boundary integral operators in acoustic and electromagnetic scattering*, Quart. J. Mech. Appl. Math., 38 (1985), pp. 323–341.

[46] G. A. Kriegsmann, A. Taflove, and K. R. Umashankar, *A new formulation of electromagnetic wave scattering using the on-surface radiation condition method*, IEEE Trans. Antennas Propag., 35 (1987), pp. 153–161.

[47] V. D. Kupradze, *Potential methods in the theory of elasticity*, Translated from the Russian by H. Gutfreund. Translation edited by I. Meroz, Israel Program for Scientific Translations, Jerusalem, 1965.

[48] V. D. Kupradze, T. G. Gegelia, M. O. Basheleĭshvili, and T. V. Burchuladze, *Three-dimensional problems of the mathematical theory of elasticity and thermoelasticity*, vol. 25 of North-Holland Series in Applied Mathematics and Mechanics, North-Holland Publishing Co., Amsterdam, russian ed., 1979. Edited by V. D. Kupradze.

[49] F. Le Louër, *A high-order spectral algorithm for elastic obstacle scattering in three dimensions*, Journal of Computational Physics, 279 (2014), pp. 1705–1733.

[50] D. P. Levadoux, *Proposition de préconditionneurs pseudo-différentiels pour l'équation cfie de l'électromagnétisme.*, M2AN, 39 (2005), pp. 147–155.

[51] D. P. Levadoux and B. L. Michielsen, *Nouvelles formulations intégrales pour les problèmes de diffraction d'ondes*, M2AN, 38 (2004), pp. 157–175.

[52] F. A. Milinazzo, C. A. Zala, and G. H. Brooke, *Rational square-root approximations for parabolic equation algorithms*, J. Acoust. Soc. Am., 101 (1997), pp. 760–766.

[53] J.-C. Nédélec, *Acoustic and electromagnetic equations*, vol. 144 of Applied Mathematical Sciences, Springer-Verlag, New York, 2001. Integral representations for harmonic problems.

[54] S. Pernet, *A well-conditioned integral equation for iterative solution of scattering problems with a variable Leontovitch boundary condition*, M2AN Math. Model. Numer. Anal., 44 (2010), pp. 781–801.

[55] V. Rokhlin, *Rapid solution of integral equations of scattering theory in two dimensions*, Journal of Computational Physics, 86 (1990), pp. 414–439.

[56] E. H. Saenger, N. Gold, and S. A. Shapiro, *Modeling the propagation of elastic waves using a modified finite-difference grid*, Wave motion, 31 (2000), pp. 77–92.

[57] O. Steinbach and W. L. Wendland, *The construction of some efficient preconditioners in the boundary element method*, Advances in Computational Mathematics, 9 (1998), pp. 191–216.

[58] R. Stevenson and R. van Venetië, *Uniform preconditioners for problems of positive order*, Computers & Mathematics with Applications, (2020).

[59] J. Virieux, H. Calandra, and R. E. Plessix, *A review of the spectral, pseudo-spectral, finite-difference and finite-element modelling techniques for geophysical imaging*, Geophysical Prospecting, 59 (2011), pp. 794–813.

[60] Y.Saad, *Iterative methods for sparse linear systems*, PWS Publishing Company, Boston, 1996.